



UNIVERSITY OF LEEDS

This is a repository copy of *Direct observation of spin-orbit splitting and phonon-assisted optical transitions in the valence band by internal photoemission spectroscopy*.

White Rose Research Online URL for this paper:
<http://eprints.whiterose.ac.uk/78951/>

Version: Published Version

Article:

Lao, Y-F, Perera, AGU, Li, LH et al. (3 more authors) (2013) Direct observation of spin-orbit splitting and phonon-assisted optical transitions in the valence band by internal photoemission spectroscopy. *Physical Review B: Condensed Matter and Materials Physics*, 88 (20). 201302. ISSN 1098-0121

<https://doi.org/10.1103/PhysRevB.88.201302>

Reuse

Unless indicated otherwise, fulltext items are protected by copyright with all rights reserved. The copyright exception in section 29 of the Copyright, Designs and Patents Act 1988 allows the making of a single copy solely for the purpose of non-commercial research or private study within the limits of fair dealing. The publisher or other rights-holder may allow further reproduction and re-use of this version - refer to the White Rose Research Online record for this item. Where records identify the publisher as the copyright holder, users can verify any specific terms of use on the publisher's website.

Takedown

If you consider content in White Rose Research Online to be in breach of UK law, please notify us by emailing eprints@whiterose.ac.uk including the URL of the record and the reason for the withdrawal request.



eprints@whiterose.ac.uk
<https://eprints.whiterose.ac.uk/>

Direct observation of spin-orbit splitting and phonon-assisted optical transitions in the valence band by internal photoemission spectroscopy

Yan-Feng Lao and A. G. Unil Perera*

Department of Physics and Astronomy, Georgia State University, Atlanta, Georgia 30303, USA

L. H. Li, S. P. Khanna,[†] and E. H. Linfield

School of Electronic and Electrical Engineering, University of Leeds, Leeds LS2 9JT, United Kingdom

H. C. Liu

Key Laboratory of Artificial Structures and Quantum Control, Department of Physics and Astronomy,

Shanghai Jiao Tong University, Shanghai 200240, China

(Received 30 January 2013; published 11 November 2013)

We employ internal photoemission spectroscopy to directly measure the valence-band Van Hove singularity, and identify phonons participating in indirect intervalence-band optical transitions. Photoemission of holes photoexcited through transitions between valence bands displays a clear and resolvable threshold, unlike previous reports of interband critical points which become obscure in doped materials. We also demonstrate the enhancement of optical phonon-assisted features primarily contributing to the photoemission yield. This result is evidence of the relaxation of photoexcited hot holes through intravalence-band scatterings in heterojunctions, which contrast with intervalence-band scatterings in bulks.

DOI: [10.1103/PhysRevB.88.201302](https://doi.org/10.1103/PhysRevB.88.201302)

PACS number(s): 78.30.Fs, 71.70.Ej, 73.40.Kp, 79.60.Jv

Optical studies of light interacting with a material reveal fundamental information about its electronic structure, photons, phonons, and carrier dynamics in the material, *inter alia*.¹⁻⁴ Many fundamental studies and device applications make use of optical transitions between different energy bands,⁵⁻¹¹ among which the valence-to-conduction band (VB to CB) transitions are typically used to determine band parameters,⁹ e.g., the interband Van Hove singularities.¹⁰ Despite the well-known electronic structure, understanding of VB-related physics is still very limited. Nearly all of what is currently understood about VBs come from optical absorption⁵⁻⁷ and interband transition-based experiments,^{9,10} the latter of which encounters a fundamental difficulty when band tailing perturbed obscuring effects dominate.¹² This limitation makes it impossible to measure the VB singularity on the basis of free-carrier effects. Aside from this, although many theoretical studies on free-carrier absorption are reported,^{13,14} the determination of the dominant contributions to the carrier-phonon coupling in indirect intervalence-band (IVB) transitions is yet to be demonstrated experimentally.

In this Rapid Communication, we demonstrate that internal photoemission (IPE) of holes at a heterojunction interface provides a direct characterization of the valence-band and hole dynamics. Of the various optical processes illustrated in Fig. 1(a), indirect transitions take place either through an intermediate state lying in the VB from which the transition originates, or through a nearby band. On the contrary to readily observing phonons associated with interband absorption in indirect-gap semiconductors,¹⁶ identifying phonons participating in indirect IVB transitions is impossible through optical absorption, according to its featureless profile [Fig. 1(b)] and also extensive absorption data reported in past literature.⁷ IPE occurs at the junction interface when the kinetic energies of photoexcited carriers in the photon absorber (emitter) are sufficiently higher than the barrier.¹⁷ For

successful photoemission, photocarriers must transfer between the energy bands of the absorber and barrier, which leads to remarkable features associated with indirect transitions due to their higher probabilities of occurring compared to direct transitions.¹⁸ Analysis of the IPE results also allows us to study hole dynamics upon photoexcitation. Our results broaden the understanding of the VBs and optical processes, which, for example, may offer a better understanding of the origin of hole-mediated ferromagnetism for *p*-type (Ga,Mn)As,¹⁹ by distinguishing IVB transitions from impurity band-to-valence band transitions through resolving the VB singularity. In addition to this fundamental interest, phonon identification will find applications in determining free-carrier absorption, an important source of modal loss in light-emitting and laser devices.^{13,14}

The IPE quantum yield (Y)¹⁷ is obtained as $Y = (I/P)h\nu$, where I is the photocurrent of the sample, and P is the power of incident light. A commercial bolometer with known sensitivity was used to measure P for spectral calibration. Photocurrent spectra were acquired by mounting the sample in a liquid-helium dewar and using a Perkin-Elmer system 2000 Fourier transform infrared (FTIR) spectrometer. The sample for IPE studies uses emitter/barrier heterojunctions (e.g., *p*-type doped GaAs/undoped AlGaAs).²⁰ Although IPE was reported more than four decades ago,²¹ it remains attractive, as recently demonstrated for characterizing materials such as graphene and oxide-based structures.²² Here, going beyond the standard focus on obtaining band offsets,^{17,21} we illustrate an exploration of IPE to study the VB structure and related optical processes.

Features of hole photoemission solely associated with the *p*-type GaAs emitter are confirmed by IPE of samples with different $\text{Al}_x\text{Ga}_{1-x}\text{As}$ barriers, as shown in Fig. 1(c). Except for the low-energy spectral end (0.1–0.3 eV) affected by the potential barrier,¹⁷ the photoemission spectra between 0.3

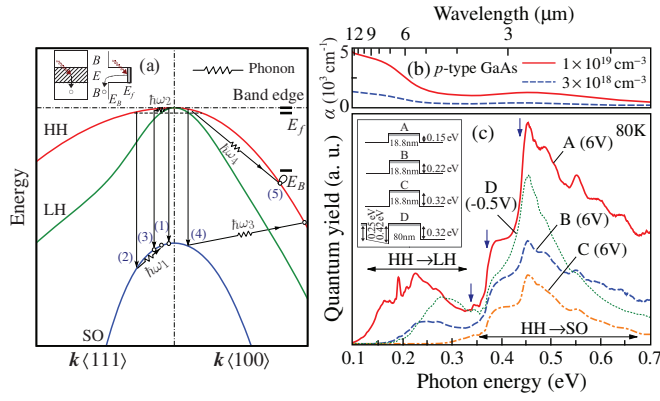


FIG. 1. (Color online) (a) Schematic of various intervalence-band (IVB) optical transitions, where (1)–(5) have the following meanings: (1) Direct IVB transition; (2) IVB transition + phonon emission ($\hbar\omega_1$); (3) phonon absorption ($\hbar\omega_2$) + IVB transition; (4) IVB transition + phonon emission ($\hbar\omega_3$) (interband scattering); and (5) phonon absorption ($\hbar\omega_4$) + intraband photon absorption. The inset shows the photon excitation and emission of a hole in an emitter (E)/barrier (B) heterojunction. It was found that transition (2) has a dominant contribution to the photoemission yield. (b) Optical absorption (α) of p -type GaAs. (c) Internal-photoemission spectra of p -type GaAs/ $\text{Al}_x\text{Ga}_{1-x}\text{As}$ heterojunctions. The inset illustrates the flat-band (VB) diagrams (Ref. 15) at zero bias. The shaded area schematically shows the Fermi level of the emitter [doping concentration: $3 \times 10^{18} \text{ cm}^{-3}$ (A, B, and C) and $1 \times 10^{19} \text{ cm}^{-3}$ (D)]. The photon energy ranges where the HH \rightarrow LH or HH \rightarrow SO transitions dominate are indicated. The features indicated by vertical arrows remain the same in different samples.

and 0.45 eV have very similar profiles between different samples. The undulations beyond 0.45 eV (samples A–C) result from optical interference which can be clarified by optical calculations. The sharp peak of sample A at 0.193 eV was previously interpreted as LH-HH spin-orbit splitting (LH and HH denote the light- and heavy-hole band, respectively).¹¹ The variation in the applied bias is to adapt to the differences in the structures between samples to obtain optimum spectra. However, the features between 0.3 and 0.45 eV barely depend on bias, as well as the barrier height and shape (affected by bias-induced image-force barrier lowering¹⁷). In comparison with absorption [Fig. 1(b)], these features likely originate from the HH \rightarrow SO hole transitions. Interband transitions and lattice absorption as the causes can be excluded, as they occur only in even higher- and lower-energy ranges, respectively. Transitions originating from the impurity band can also be excluded, because the impurity band is already merged with the VB for doping concentration of $> 3 \times 10^{18} \text{ cm}^{-3}$.⁸ Moreover, the intravalence-band transition is insignificant for this spectral range. This leaves the intervalence-band transitions as the only mechanism for interpreting the features.

In order to examine the features in more detail, we differentiated quantum yield spectra [Figs. 2(a)–2(c)]. The peaks in the double differential plots correspond to the onsets of these features, and are thus used to determine thresholds of various transitions. It is tempting to interpret the second derivative peak at ~ 0.34 eV as correlated with the HH \rightarrow SO singularity, corresponding to the band splitting gap at the Γ point (Δ_0). This assertion is clarified by calculating

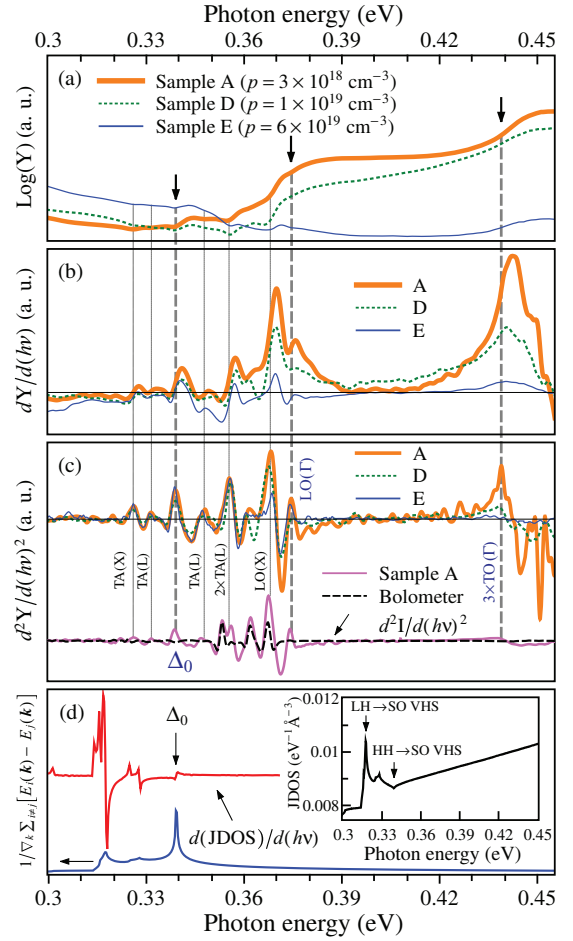


FIG. 2. (Color online) Comparison of (a) quantum yield (Y), and its (b) first and (c) second derivatives for samples A (6 V, 80 K), D (-0.5 V, 80 K), and E (0.05 V, 50 K). The structure of sample E is the same as A, except for its emitter doping concentration ($6 \times 10^{19} \text{ cm}^{-3}$). The vertical lines indicate the identified phonon features (Table I). Also shown in (c) are the second derivatives of the as-measured sample and bolometer (background) spectra. (d) Calculated $1/\sqrt{k} \sum_{i,j} [E_i(\mathbf{k}) - E_j(\mathbf{k})]$ by a $\mathbf{k} \cdot \mathbf{p}$ model (Ref. 23) to show the Van Hove singularities (VHS) of intervalence-band transitions, two of which are indicated in the inset. Also shown is the derivative of JDOS.

$1/\sqrt{k} \sum_{i,j} [E_i(\mathbf{k}) - E_j(\mathbf{k})]$ to show the singularities, and the joint density of states (JDOS), as illustrated in Fig. 2(d). The quantum yield can be expressed as¹⁷

$$Y(h\nu) \sim \int_{\Delta-h\nu}^{\infty} \rho(\epsilon, E_f) f(\epsilon) P(\epsilon + h\nu, \Delta) d\epsilon, \quad (1)$$

where ρ and P are the energy distribution of photoexcited holes and their escape probability, respectively. E_f is the Fermi level. $f(\epsilon)$ is the Fermi-Dirac distribution function. As f and P are slowly varying functions (in the energy regime around Δ_0), we take the dominant contribution of ρ for calculating derivatives, i.e., $dY/d(h\nu) \sim \rho(\Delta - h\nu, E_f)$, and hence $d^2Y/d(h\nu)^2 \sim d(\text{JDOS})/d(h\nu)$, where ρ takes the line shape of JDOS if only direct IVB transitions are considered. The LH \rightarrow SO transition exhibits a strong saddle-point singularity but cannot be observed because of the lower hole occupancy in the LH band. Due to its three-dimensional nature

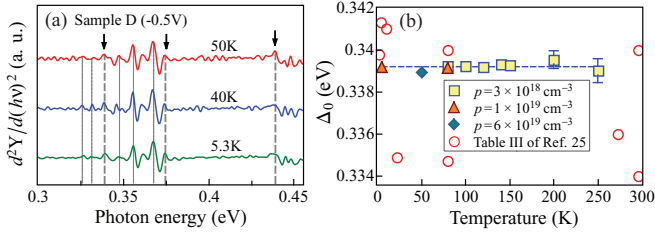


FIG. 3. (Color online) (a) Second yield derivative spectra of sample D at different temperatures. Results at different biases are similar and thus not shown here. Vertical lines indicate the identified phonon features. (b) Temperature and doping dependence of Δ_0 for GaAs which nearly remain constant (dashed line). Data of Δ_0 adopted from Table III of Ref. 25 are shown for comparison.

(dipole forbidden at Γ), the HH \rightarrow SO singularity shows a weak signature in $d(\text{JDOS})/d(h\nu)$, in consistence with the experimental feature of $d^2Y/d(h\nu)^2$. As shown in Fig. 2(c), a quite smooth as-measured bolometer spectrum around Δ_0 justifies this result as not due to the background.

Typically, Δ_0 was *indirectly* determined^{10,24} through resolving interband critical points (at Γ): E_0 (HH to CB transitions) and $E_0 + \Delta_0$ (SO to CB). *Direct* determination of Δ_0 enables the study of its dependence on the doping concentration (Fig. 2) and temperature [Fig. 3(a)]. The determined values plotted in Fig. 3(b) indicate that Δ_0 nearly remains unchanged, and has an average of 0.3392 ± 0.0003 eV, in reasonable agreement with reported values which are believed to be closer to 0.390–0.341 eV.^{26,27} While the temperature dependency of Δ_0 can be readily obtained from interband transitions of undoped GaAs, it is difficult to determine the doping dependency,¹² as band tailing significantly perturbs the density of states (DOS) at Γ . It can be deduced according to the two-thirds rule [$\Delta_1 = (2/3)\Delta_0$],²⁸ that Δ_0 remains constant, as interband critical points E_1 (HH to CB) and $E_1 + \Delta_1$ (LH to CB) (at larger k) synchronously vary with doping concentrations.²⁹ Our experiment is a direct justification of this result.

Band tailing introduces extended states in both the CB and VB, notably causing a reduction of the effective band gap.

Likewise, the expected reduction of the SO-HH splitting gap would be about 13 meV for $p = 1 \times 10^{19} \text{ cm}^{-3}$. However, stationary Δ_0 is confirmed in this study, indicating that Δ_0 is free of the shrinkage due to carrier-induced exchange and correlation effects³⁰ as in the band gap. The unaltered HH \rightarrow SO singularity may originate from transitions through localized states owing to dopants caused potential fluctuations. This supports the rigidity of the VBs, of which only the temperature rigidity has been studied previously.³¹ Our findings justify the rigid-band argument for studies, such as understanding doping-induced band gap narrowing effects and band alignment of doped heterojunctions.¹⁷

Returning to the phonon study, we identify phonons participating in IVB transitions based on yield spectra, and use the second derivatives to determine their energies. The possibility for the occurrence of indirect transitions is partially supported by observing a nonvanishing yield around Δ_0 . Calculations¹⁴ have shown enhanced absorption by over an order of magnitude, as a consequence of diverted transitions at large k points (dipole allowed) to $k = 0$ (dipole forbidden) where the hole occupation is very strong. The participation of phonons plays an important role in this process; each of them results in an individual threshold being resolved. Noticing that IVB absorption is broad and featureless [Fig. 1(b)], the featured yield is thus a result of enhancement due to phonon-assisted transitions. The strongest features at ~ 0.37 and 0.44 eV [Fig. 2(a)], which can be exclusively distinguished compared to the background [Fig. 2(c)], are assigned with the energies of $\Delta_0 + E_{\text{ph}}$, i.e., correlating with phonons: LO(Γ) and $3 \times$ TO(Γ) (E_{ph} is the phonon energy). It was found that, as shown in Fig. 2(a), these two features diminish as the emitter doping concentration increases to a higher level (sample E). Enhanced scatterings by charged impurity centers, as observed in the broadening of HH \rightarrow SO absorption,⁷ may alleviate the carrier-phonon coupling and cause yield reduction. Such an effect is in support of observed phonon features.

Identification of other phonons associated with relatively weaker features may need good differentiation between the sample and background signal. As shown in Fig. 2(c), the only suspicious feature is LO(X). Although this is also shown in

TABLE I. IPE features associated with phonons of GaAs (80 K). Δ_0 is the HH-SO spin-orbit splitting energy with a value of 339.2 ± 0.3 meV. The energies of single phonons are the averages of values from different samples measured at different experimental conditions. The numbers in parentheses are uncertainties.

Features (meV)	$\Delta_0 - 13.0$	$\Delta_0 - 7.4$	Δ_0	$\Delta_0 + 8.7$	$\Delta_0 + 16.3$
Phonons	TA(X)	TA(L)		TA(L)	$2 \times$ TA(L)
Features (meV)	$\Delta_0 + 28.9$	$\Delta_0 + 35.4$	$\Delta_0 + 99.4$		
Phonons	LO(X)	LO(Γ)	$3 \times$ TO(Γ)		
	TO(Γ)	LO(Γ)	LO(X)	TA(X)	TA(L)
This work (meV)	33.1(0.2)	35.4(0.2)	28.9(0.2)	12.2(0.8)	8.1(0.5)
Waugh <i>et al.</i> ^a	33.2(0.3)	35.4(0.8)	29.9(0.6)	9.75(0.06)	7.70(0.06)
Blakemore ^b	33	35.5	30	8	
Giannozzi <i>et al.</i> ^c	33.6	36.1	29.8	10.2	7.8
Steiger <i>et al.</i> ^d	33.2	36.1	28.9	8.9	8.8

^aReference 32.

^bExtracted from multiple phonon assignment to reststrahlen absorption peaks; see Table XI of Ref. 27.

^cReference 33.

^dReference 34.

the as-measured background spectrum, its existence cannot be ruled out as its normalized intensity is much higher than that of the background. Various phonons that were determined are shown in Table I. High-energy phonon features are interpreted as multiples of the same phonon rather than a combination of different phonons, as this assignment gives the best agreement with previously reported values.^{27,32–34} Due to a small expected variation, no temperature effect on the phonon energy can be identified.³⁵ As the phonon emission rate decreases, the quantum yield decreases at higher temperatures. However, deducing the temperature dependency of the phonon features is not straightforward because photoemission efficiency is also affected by photon absorption and hole escape probability. The nonvanishing phonon-absorption peaks at 5.3 K [Fig. 3(a)] are thought to be due to hole thermalization,³⁶ which provides necessary phonons for assisting the photoemission of holes.²⁰ A similar absorption of acoustic phonons is observed at 1.5 K, when phonons are generated by a heater.³⁷

Attention should be paid to the most important phonons, $LO(\Gamma)$ and $3 \times TO(\Gamma)$, which have the most significant contributions to the yield. This agrees with previous studies on the dominant hole-optical phonon interactions.³⁸ Our result is an experimental validation for the theoretical evaluation of phonon-assisted IVB absorption, for which a theoretical model is typically employed to predict the role of phonons, with justification from other experiments.¹³ The major role of $3 \times TO(\Gamma)$ instead of one TO phonon, although confirmed experimentally, remains to be explained, which may require further study based on this observation.

We confirm the hot-hole dynamics of Fig. 4(a) for heterojunctions. As photoexcited hot holes tend to relax to the top of the VB, an intervalence-band scattering typically occurs to enable the transfer of a hot hole between different bands [Fig. 4(b)], which is then followed by intraband hole-hole or hole-phonon scatterings for further relaxation, as reported

TABLE II. Comparison of Δ_0 of GaAs, $In_{0.53}Ga_{0.47}As$, and GaSb with reported values. The numbers in parentheses are uncertainties.

	GaAs	$In_{0.53}Ga_{0.47}As$	GaSb
This work (meV)	339.2(0.3)	332.8(0.3)	794.8(0.03)
Reported values (meV)	390–341 ^a	329.6 ^b	796 ^c

^aReferences 26 and 27.

^bVurgaftman *et al.* (Ref. 26).

^cMuñoz *et al.* (Ref. 24).

in bulks.³⁹ Hole-hole scatterings proceed in a fast time scale and dominate in the intraband (HH) relaxation. In the heterojunction case, this leads to a higher-order relaxing process compared to Fig. 4(a), due to required additional scattering to facilitate the escape of a hot hole over a potential barrier. The relaxing picture of Fig. 4(a) depicts relaxation towards to the SO top instead of the HH, correlating with observations that confirm phonon features associated with the $HH \rightarrow SO$ singularity. The potential barrier diverts the relaxation channel primarily through the SO band, which principally contributes to the yield outcome. Such a mechanism was also found in quantum-dot structures,⁴⁰ where carriers in the wetting layer with low kinetic energy (near the Γ point) are scattered into quantum dots.

The photoemission study was extended to inspect Δ_0 of GaSb (Ref. 20) and $In_{0.53}Ga_{0.47}As$, as shown in Figs. 4(c) and 4(d), respectively. The values of Δ_0 (Table II) are obtained as 794.8 ± 0.03 meV (GaSb) and 332.8 ± 0.3 meV ($In_{0.53}Ga_{0.47}As$), which agree with the reported values of 796 meV (GaSb)²⁴ and 329.6 meV ($In_{0.53}Ga_{0.47}As$).²⁶ The identified feature is also confirmed by observing an onset of the yield (a change in the slope). It is thus found that the second derivative peak at 365.4 meV for $In_{0.53}Ga_{0.47}As$ [Fig. 4(d)] corresponds to the GaAs-like $LO(\Gamma)$ phonon (32.6 meV), in agreement with the value of 33.3 meV reported by Adachi.⁴¹ The feature associated with the InAs-like phonon cannot be confirmed, probably due to much weaker coupling between the carrier and InAs-like phonon, compared to that between the carrier and GaAs-like phonon, as confirmed by optical reflection.⁴²

In conclusion, we have directly measured valence-band spin-orbit splitting and determined phonons participating in IVB indirect transitions by using IPE spectroscopy. The VB splitting energy of GaAs was found to remain unchanged, although degenerate doping introduces appreciable band tailings. The major role of optical phonons in IVB processes is confirmed, providing experimental validation for evaluating free-carrier IVB absorption. IPE results also indicate the hot-hole dynamics in heterojunctions with dominant relaxation through intravalence-band scatterings.

This work was supported in part by the US Army Research Office under Grant No. W911NF-12-2-0035 monitored by William W. Clark, and in part by the US National Science Foundation under Grant No. ECCS-1232184. The University of Leeds acknowledges supports from the UK Engineering and Physical Sciences Research Council, and E.H.L. from the European Research Council Advanced Grant “TOSCA.”

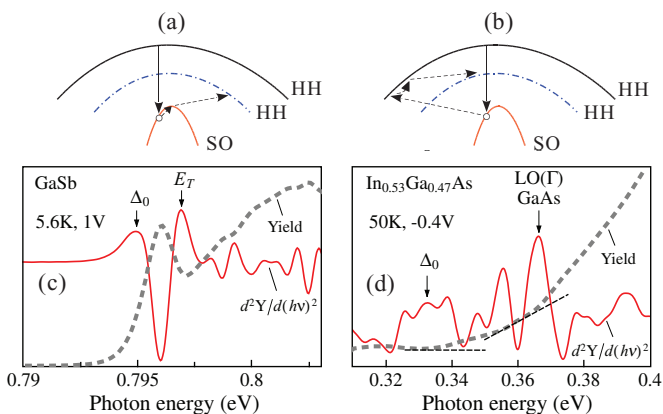


FIG. 4. (Color online) (a) and (b) are schematics of hole transitions (vertical lines) and scattering processes (dashed lines), corresponding to the hot-relaxation pictures obtained in this study and reported by Ref. 39, respectively. The energy bands plotted with solid and dashed-dotted lines are for the emitter and barrier, respectively. Spectral yield and second yield derivatives for (c) p -type GaSb/GaSb and (d) p -type InGaAs/InGaAsP/InP junctions. E_T corresponds to transitions across the band gap of GaSb (Ref. 20). The dashed straight line crossing with the yield spectrum is to show the location where the slope is about to change.

H.C.L. is thankful for support from the National Major Basic Research Projects (2011CB925603) and the Natural Science Foundation of China (91221201). H.C.L. supported this work in all aspects, including carrying out the device processing,

reading and commenting the manuscript, until his death in October 2013. The authors also acknowledge Vadym Apalkov and Ramesh Mani for reading the manuscript and for fruitful discussions.

*uperera@gsu.edu

[†]Present address: Physics of Energy Harvesting, CSIR-National Physical Laboratory, New Delhi 110012, India.

¹Z. Fei, A. S. Rodin, G. O. Andreev, W. Bao, A. S. McLeod, M. Wagner, L. M. Zhang, Z. Zhao, M. Thiemens, G. Dominguez, M. M. Fogler, A. H. C. Neto, C. N. Lau, F. Keilmann, and D. N. Basov, *Nature (London)* **487**, 82 (2012).

²N. M. Gabor, J. C. W. Song, Q. Ma, N. L. Nair, T. Taychatanapat, K. Watanabe, T. Taniguchi, L. S. Levitov, and P. Jarillo-Herrero, *Science* **334**, 648 (2011).

³S. J. Moon, A. A. Schafgans, M. A. Tanatar, R. Prozorov, A. Thaler, P. C. Canfield, A. S. Sefat, D. Mandrus, and D. N. Basov, *Phys. Rev. Lett.* **110**, 097003 (2013).

⁴Z. Li, E. A. Henriksen, Z. Jiang, Z. Hao, M. C. Martin, P. Kim, H. Stormer, and D. N. Basov, *Nat. Phys.* **4**, 532 (2008).

⁵T. Jungwirth, P. Horodyská, N. Tesařová, P. Němec, J. Šubrt, P. Malý, P. Kužel, C. Kadlec, J. Mašek, I. Němec, M. Orlita, V. Novák, K. Olejník, Z. Šobáň, P. Vašek, P. Svoboda, and J. Sinova, *Phys. Rev. Lett.* **105**, 227201 (2010).

⁶K. S. Burch, D. B. Shrekenhamer, E. J. Singley, J. Stephens, B. L. Sheu, R. K. Kawakami, P. Schiffer, N. Samarth, D. D. Awschalom, and D. N. Basov, *Phys. Rev. Lett.* **97**, 087208 (2006).

⁷See, for example, R. Newman and W. W. Tyler, *Phys. Rev.* **105**, 885 (1957); R. Braunstein and L. Magid, *ibid.* **111**, 480 (1958).

⁸B. C. Chapler, R. C. Myers, S. Mack, A. Frenzel, B. C. Pursley, K. S. Burch, E. J. Singley, A. M. Dattelbaum, N. Samarth, D. D. Awschalom, and D. N. Basov, *Phys. Rev. B* **84**, 081203 (2011).

⁹T. de Boer, A. Gamouras, S. March, V. Novák, and K. C. Hall, *Phys. Rev. B* **85**, 033202 (2012).

¹⁰M. Cardona, K. L. Shaklee, and F. H. Pollak, *Phys. Rev.* **154**, 696 (1967).

¹¹Y. F. Lao, P. K. D. D. P. Pitigala, A. G. U. Perera, H. C. Liu, M. Buchanan, Z. R. Wasilewski, K. K. Choi, and P. Wijewarnasuriya, *Appl. Phys. Lett.* **97**, 091104 (2010).

¹²For example, Ref. 10 reported various interband critical points at different doping concentrations, except for E_0 and $E_0 + \Delta_0$ at the Γ point, at which doping-caused potential fluctuations perturb the band edge states.

¹³E. Kioupakis, P. Rinke, A. Schleife, F. Bechstedt, and C. G. Van de Walle, *Phys. Rev. B* **81**, 241201 (2010).

¹⁴M. Takeshima, *Phys. Rev. B* **32**, 8066 (1985); A. Haug, *Semicond. Sci. Technol.* **5**, 557 (1990).

¹⁵J. Batey and S. L. Wright, *J. Appl. Phys.* **59**, 200 (1986).

¹⁶J. Noffsinger, E. Kioupakis, C. G. Van de Walle, S. G. Louie, and M. L. Cohen, *Phys. Rev. Lett.* **108**, 167402 (2012); A. Frova and P. Handler, *ibid.* **14**, 178 (1965).

¹⁷Y. F. Lao and A. G. Unil Perera, *Phys. Rev. B* **86**, 195315 (2012).

¹⁸R. J. Powell, *J. Appl. Phys.* **41**, 2424 (1970).

¹⁹N. Samarth, *Nat. Mater.* **11**, 360 (2012).

²⁰See Supplemental Material at <http://link.aps.org/supplemental/10.1103/PhysRevB.88.201302> for information about sample structures, fabrication, and characterization. The photoemission study on GaSb is described.

²¹V. Afanas'ev, *Internal Photoemission Spectroscopy: Principles and Applications* (Elsevier, Amsterdam, 2010).

²²K. Xu, C. Zeng, Q. Zhang, R. Yan, P. Ye, K. Wang, A. C. Seabaugh, H. G. Xing, J. S. Suehle, C. A. Richter, D. J. Gundlach, and N. V. Nguyen, *Nano Lett.* **13**, 131 (2013); Y. Hikita, M. Nishikawa, T. Yajima, and H. Y. Hwang, *Phys. Rev. B* **79**, 073101 (2009).

²³T. B. Bahder, *Phys. Rev. B* **41**, 11992 (1990).

²⁴M. Muñoz, K. Wei, F. H. Pollak, J. L. Freeouf, and G. W. Charache, *Phys. Rev. B* **60**, 8105 (1999).

²⁵P. Lautenschlager, M. Garriga, S. Logothetidis, and M. Cardona, *Phys. Rev. B* **35**, 9174 (1987).

²⁶A. G. Thompson, M. Cardona, K. L. Shaklee, and J. C. Woolley, *Phys. Rev.* **146**, 601 (1966); I. Vurgaftman, J. R. Meyer, and L. R. Ram-Mohan, *J. Appl. Phys.* **89**, 5815 (2001).

²⁷J. S. Blakemore, *J. Appl. Phys.* **53**, R123 (1982).

²⁸E. O. Kane, *J. Phys. Chem. Solids* **1**, 82 (1956).

²⁹M. Kuball, M. K. Kelly, M. Cardona, K. Köhler, and J. Wagner, *Phys. Rev. B* **49**, 16569 (1994).

³⁰Y. Zhang and S. Das Sarma, *Phys. Rev. B* **72**, 125303 (2005).

³¹D. Auvergne, J. Camassel, H. Mathieu, and M. Cardona, *Phys. Rev. B* **9**, 5168 (1974).

³²J. L. T. Waugh and G. Dolling, *Phys. Rev.* **132**, 2410 (1963).

³³P. Giannozzi, S. de Gironcoli, P. Pavone, and S. Baroni, *Phys. Rev. B* **43**, 7231 (1991).

³⁴S. Steiger, M. Salmani-Jelodar, D. Areshkin, A. Paul, T. Kubis, M. Povolotskyi, H.-H. Park, and G. Klimeck, *Phys. Rev. B* **84**, 155204 (2011).

³⁵The maximum operating temperature in our experiments is 250 K; however, as a result of spectral noise, phonon features can only be resolved up to 140 K, at which the energy of LO phonon is only 0.2 meV less than that at 0 K. Such a small variation is within the uncertainty of measurements and thus not identifiable.

³⁶B. Brill and M. Heiblum, *Phys. Rev. B* **49**, 14762 (1994); S. Hunsche, H. Heesel, A. Ewertz, H. Kurz, and J. H. Collet, *ibid.* **48**, 17818 (1993).

³⁷A. J. Kent, R. E. Strickland, K. R. Strickland, and M. Henini, *Phys. Rev. B* **54**, 2019 (1996).

³⁸M. Heiblum, D. Galbi, and M. Weckwerth, *Phys. Rev. Lett.* **62**, 1057 (1989); Q. O. Hu, E. S. Garlid, P. A. Crowell, and C. J. Palmström, *Phys. Rev. B* **84**, 085306 (2011); D. C. Tsui, *Phys. Rev. Lett.* **21**, 994 (1968).

³⁹M. Woerner, T. Elsaesser, and W. Kaiser, *Phys. Rev. B* **45**, 8378 (1992).

⁴⁰J. Wolters, M.-R. Dachner, E. Malić, M. Richter, U. Woggon, and A. Knorr, *Phys. Rev. B* **80**, 245401 (2009).

⁴¹S. Adachi, P. Capper, S. Kasap, and A. Willoughby, *Properties of Semiconductor Alloys: Group-IV, III-V and II-VI Semiconductors* (Wiley, Hoboken, NJ, 2009).

⁴²M. Amiotti, G. Guizzetti, M. Patrini, A. Piaggi, A. Borghesi, L. Colombo, and G. Landgren, *J. Appl. Phys.* **75**, 3085 (1994).